IJFANS INTERNATIONAL JOURNAL OF FOOD AND NUTRITIONAL SCIENCES
ISSN PRINT 2319 1775 Online 2320 7876
Research Paper © 2012 IJFANS. All Rights Reserved UGC CARE Listed (Group -I) Journal Volume 11, Iss 13, 2022

A REMUNERATIVE CHEMICAL STRATEGY FOR SYNTHESIZING PHOTCATALYTIC SIGNIFICANT AMORPHOUS SILICA NANOPARTICLES UTILIZING CASSAVA PERIDERM ASH

Aashikha Shani R.S[1], Ambrose Rejo Jeice[2,*]

[1]Research Scholar (Reg No.: 22113012132002), Department of Physics & Research Centre, Annai Velankanni College, Tholayavattam, Kanyakumari District, Affiliation to Manonmaniam Sundaranar University, Abishekapatti, Tirunelveli 627012, Tamilnadu, India.

[2,*]Department of Physics & Research Centre, Annai Velankanni College, Tholayavattam, Kanyakumari District, Affiliation to Manonmaniam Sundaranar University, Abishekapatti, Tirunelveli 627012, Tamilnadu, India.Email: rejojeice@gmail.com

ABSTRACT

Blazing and discarding of agricultural waste negligently besmirches the environment and increases greenhouse gas emissions. The abundance and renewable nature of agricultural wastes have prompted researchers to delve into re purposing discarded materials into utility items. The amount of agricultural waste generated has steadily risen in recent years as a consequence of the food supply chain's heightened efficiency. Legion researchers have taken cognizance of recent developments in the synthesis of Silica nanoparticles (SNP) from agricultural waste made from cassava periderm ash (CPA) and their application in the removal of various customary environmental contaminants from water. SNPs can have their configuration, appearance, porosity, and size revamped by adjusting the processing parameters during synthesis. Researchers are looking at these characteristics along with the associated uses of SNPs to figure out if agricultural waste may be leveraged to make silica precursors. The isolation of high-purity SiO_2 from cassava (Manihot esculenta) periderm ash was achieved via an alkaline-precipitation method, evaluating the effects of calcination temperature (650 °C and 750 °C) and NaOH concentration (3 N, 5 N) on yield and performance which was characterized by XRD (amorphous phase confirmation), SEM-EDX (morphology, purity), FTIR (Si–O–Si and Si–OH vibrations), BET surface area and UV–Vis spectroscope. Silica from CPA employed for photocatalytic methyl orange degradation, 70 % of the dye was broken down in 90 minutes. These results establish optimal conditions for converting cassava periderm waste into functional SiO_2 capable of efficient organic dye removal.

KEYWORDS: Silica nanoparticles, Photocatalytic application, Methyl Orange, Precipitation method, Cassava Periderm

INTRODUCTION

One of the most extensively studied materials in contemporary science, silica nanoparticles (SNPs) are now often used in surface coatings, biomedicine, catalysis, and the manufacture of new self-assembling materials. Developing a basic grasp of SNP characteristics and behavior is greatly aided by theoretical techniques. Modeling silica structure, the silica-water interfaces, as well as functionalizing silica surfaces for specific purposes, are areas of intense scientific interest [1]. Researchers have been interested in silica nanoparticles because of their special properties, which include large surface area, pore volume, variable pore size, great

Research Paper © 2012 IJFANS. All Rights Reserved

biocompatibility, the capacity to encapsulate both hydrophilic and hydrophobic molecules, and scalable synthetic availability [2]. Numerous techniques, including biodigestion, precipitation, sol-gel, strong acid leaching, microwave heating, fluidized bed, and carboxylic acid leaching, can be used to produce pure silica from tropical agricultural waste [3].

One of the most extensively researched substances in science and engineering is silica, often known as silicon dioxide, or SiO_2. Although it comes in a wide variety of crystalline and amorphous forms, it is most frequently found as quartz or sand [4]. For thousands of years, crystalline silica has been used to make glass and concrete. More recently, it has been used to make refractory materials and high-temperature ceramics. Four O atoms coordinate Si in crystalline silica, and each O forms a link with two Si atoms. This creates a network of interconnected tetrahedra with bridging O atoms and center Si atoms [5]. Certain peculiar physical characteristics of molten or liquid silica are similar to those of water. Similar to water, silica exhibits negative temperature expansion, wherein cooling causes both molecules to develop crystalline structures, leading to a less dense system. When most materials cool and freeze, they grow denser. Less kinetic energy allows cooler molecules to disperse and elude each other's attraction. However, when the molecules of silica and water become less kinetic, they form crystalline formations. This means that the structure as a whole holds more space, leading to a decrease in density [6, 8]. The piezoelectric effect is another characteristic that silica, like quartz, exhibits. Certain crystals, such as quartz, have partially symmetrical molecular crystalline structures, which give rise to the piezoelectric effect [7]. Nonetheless, the configuration of the atoms and the electrons they share leads to an electrostatic charge that is precisely balanced. Because silicon and oxygen are polarly covalently linked, silicon exchanges electrons unevenly. Because oxygen is more electronegative than silicon, it exerts a greater pull on the electrons that are shared by both elements. As a result, the silicon atom has an overall positive charge, while the oxygen atoms in silica have a tiny negative charge [9].

Despite the tiny charges that the atoms in the silica have, the crystalline structure's total charge is neutral as the atoms are close enough to cancel each other out. Squeezing a quartz crystal, however, causes the crystalline structure to be distorted. As a result, the structure's many electrostatic charges overlap and stretch past one another. As a result, the net charge ceases to be neutral, although voltage is still possible since the crystal's opposite ends contain opposing charges [10]. Commercially available high-purity silica is very expensive to utilize and, due to its high melting point, is not appropriate for the majority of industrial uses. Since SiO_2 raw materials may be used for a variety of purposes, several different approaches have been investigated to synthesize them [11].

Because of its edible, starchy, tuberous root, cassava (Manihot esculenta), commonly known as manioc or tapioca root, is grown as an annual crop in tropical and subtropical countries [12]. Tapioca is a powdered extract made from dried cassava. In the tropics, cassava ranks third in terms of dietary carbohydrate content, after maize and rice. More than half a billion people rely on cassava as a staple crop in the developing countries [13]. It can thrive on marginal soils and is among the most drought-tolerant crops. Both the sweet and bitter types of cassava include toxins and antinutritional elements, much as other roots and tubers do. It needs to be cooked correctly before eating [14]. Acute cyanide toxicity, goiters, ataxia, and

partial paralysis can result from improperly prepared cassava, which can leave enough residual cyanide [15]. More than 500 million people rely on cassava, which is a staple meal in the tropics and the third-largest source of carbohydrates in diets after rice and maize. It has the benefit of being incredibly resistant to drought and thriving on subpar soil. Thailand is the biggest exporter of cassava starch, whereas Nigeria is the biggest producer [16]. The storage root is the portion of a cassava plant that is harvested. This has a rough brown rind that is easily separated, and it is long and tapering. The texture of the white or yellowish meat is uniform and solid [17]. A woody vascular bundle runs along the middle of commercial cultivars, which can measure 5 to 10 centimeters (2 to 4 inches) broad at the top and 15 to 30 centimeters (6 to 12 inches) long. With trace levels of calcium (16 mg/100 g), phosphorus (27 mg/100 g), and vitamin C (20.6 mg/100 g), the tuberous roots are mostly composed of starch [18]. With the exception of being deficient in methionine, an important amino acid, cassava roots have little protein, whereas their leaves are abundant in it. Both human consumption and industrial uses are found in India, where a sizable amount of the crop is utilized to make chips, sago, and starch [19]. In some areas, it's also utilized as animal feed and as a staple meal. Particularly in Kerala, Tamil Nadu, Andhra Pradesh, and the northeastern regions, cassava is eaten as a secondary staple, frequently with rice [20]. A significant amount of the cassava crop is used to extract starch, which is then used in a variety of businesses. Paper, Adhesives, and Textiles: Paper, glue, and textiles are all made from cassava starch. Food and Pharmaceutical Industries also utilizes Cassava [21]. In order to extract silica nanoparticles from CPA, we use acid precipitation in this work. We subsequently use a range of characterisation techniques to evaluate the structure, shape, purity, and yield of these particles. The primary objectives of this project are to create a highly efficient photocatalytic absorbent from CPA that will aid in the degradation of certain organic dyes in polluted water. Furthermore, this study aims to create the absorbent utilizing green synthesis techniques with CPA, a silica resource that is economically feasible. This study may show an applicable approach for creating silica nanoparticles with outstanding resilience and photocatalytic destruction.

Fig.1: Pictorial representation of the synthesis process of silica from Cassava Periderm ash

Research Paper © 2012 IJFANS. All Rights Reserved

2.1 SAMPLE PREPARATION

Cassava Periderm was collected from farm lands of kanyakumari district. Initially, the Cassava were cleaned by water to remove the dirt and dried at sunlight for two days. The cleaned periderm was now uncontrollably burned in open environment. The burnt periderm ash was collected and it was calcined under temperature at 650 ºC for 2 hours [22].

2.2 SYNTHESIS PROCESS

A predefined weight of Cassava Periderm ash (CPA) is taken into account. For a period of time at 70 °C, stir the ash with 100 ml of a 3N and 5N NaOH solution. Filter the mixture after stirring, and then rinse the residue with 20 ml of hot water. Let the filtrate cool to room temperature altogether. Employing the titration technique, the sodium silicate solution is infused with 5N H_2SO_4 solution while being continuously stirred at 70 ºC. When the pH of the acidic solution reaches 2, silica has completely precipitated out of the sodium silicate solution. To extract the micro silica, the filtrate should be dried at 100 ºC for 20 hours after being rinsed with distilled water to eliminate sulphate impurities. To get rid of the acid, the end outcome is continually washed with distilled water. After that, the solution is treated with concentrated H_2SO_4 until a white precipitate forms. After continuously washing the precipitated solution with warm water until the filtrate is entirely free of alkali, the procedure is repeated with distilled water, and the filtrate is dried in an oven heated at 100 ºC for 35 hours. The powder sample is annealed at 650 ºC and 750 ºC in the end resulting fine white powdered nanosilica [23].

2.3 CONTROL AND OPTIMIZATION OF VARIOUS PARAMETERS TO SYNTHESIZE SILICA NPS

The dilution ratios of CPA to NaOH solution, alongside the temperatures of incubation, calcination, and duration, were found to impact the synthesis of silica nanoparticles. These factors were measured and tweaked to produce silica nanoparticles swiftly and effectively. Following experiments involving different concentrations, 3N and 5N were found to be the ideal NaOH concentrations. The incubation period and calcination temperatures (650 and 750 ºC) were crucial in improving the crystallite structure and diminishing the contaminants. Silica-based materials are frequently modified by alkali treatment with NaOH, which affects porosity, surface area, and crystallinity. The produced silica samples were treated with 3N and 5N NaOH solutions to analyze their structural and chemical changes.

3. CHARACTERIZATION

To investigate the chemical and structural properties of raw biomass fuels and their combustion-derived ashes, a series of advanced analytical techniques were employed. FTIR analysis was conducted using an IRTracer-100 spectrometer to identify key organic functional groups and compounds. The spectra were recorded in the 400–4000 cm^{-1} range with a high resolution of 1 cm^{-1}, allowing for precise detection of molecular vibrations. The Brunauer-Emmett-Teller (BET) method was applied to determine the specific surface area by analyzing nitrogen adsorption isotherms at 77 K. The measurements were performed in the relative pressure range (p/p_0) of 0.05–0.3, with nitrogen's molecular cross-sectional area taken as 0.162 nm^2. The total pore volume was assessed at $p/p_0 = 0.98$, while nonlocal density functional theory (NLDFT) was used to evaluate pore size distribution via a Micromeritics ASAP PLUS system. Photocatalytic activity was evaluated using a high-

Research Paper © 2012 IJFANS. All Rights Reserved

pressure mercury lamp (GGZ300, Shanghai Jiguang) with an irradiance of 23 mW/cm². The degradation of Methyl Orange (MO) dye was monitored using a TU-1950 UV-Vis spectrophotometer (Beijing Puxi), measuring absorbance at 464 nm before and after irradiation. Field-Emission Scanning Electron Microscopy (FE-SEM) (A JSM-7800) operated at 3 kV provided high-resolution images of sample morphology. Crystalline phases were analyzed using a D8 Advance ECO diffractometer (Kalasalingam Academy of Research and Education) with Cu-Kα radiation. Scans were performed from 10° to 80° (2θ) at a step size of 0.06° and a scan rate of 4°/min. By using UV-Vis-NIR Spectroscopy diffuse reflectance spectra were obtained using a spectrophotometer (Kyoto, Japan) equipped with an integrating sphere, covering 200–800 nm with $BaSO_4$ serving as the reflectance standard. This integrated approach facilitated a comprehensive understanding of the physicochemical properties of CPA, along with their potential applications in photocatalysis.

3.1 PHOTOCATALYTIC ACTIVITY

The degradation of a MO dye solution with an initial concentration of 50 mg/L under visible light irradiation was tested in order to assess the photocatalytic efficacy of the nanoparticle photocatalysts. In the photocatalysis, 30 mL of aqueous MO dye solution was mixed with 30 mg of photocatalyst while being constantly stirred. Prior to irradiation, the dye solution containing the photocatalyst was agitated and left in the dark to achieve adsorption–desorption equilibrium. A space of 10 cm was maintained between the reactor and the bulb. Under 0 W UV lamp irradiation, the photocatalytic performance of SiO_2 samples with different calcination temperatures was examined. In the meanwhile, Silica from CPA photocatalyst samples' photocatalytic performance was assessed using a 10 W visible Florescence lamp. The sample of dye solution was taken every 30 minutes on average. In order to separate the photocatalyst particles, the obtained sample was centrifuged right away for 10 minutes at 8200 rpm. Lastly, the UV-Vis spectrophotometer was used to determine the absorbance of the liquid supernatant. For measuring the MO concentration, using the wavelength of maximum absorption, which is 464 nm. The MO dye solutions' absorption spectra were recorded every 30 minutes on average [24]. The proportion of the dye concentration that remained above the original dye concentration, as determined by the absorbance standard curve, was used to report the rate of degradation. The disposal percentage (%R) of methyl Orange dye utilizing the CPA at 650 ºC and 750 ºC adsorbents was expressed below.

$$R = \frac{C_0 - C_e}{C_O} * 100$$

where, C_o is the initial concentration of methyl orange (mg/L) and C_e is the equilibrium concentration of methyl orange dye (mg/L). The disposal capability (Q, mg/g) of the CPA at 650 ºC and 750 ºC adsorbents towards methyl orange dye was expressed below.

$$Q = C_0 - C_e \times \frac{V}{W}$$

where, W is the weight of the CPA at 650 ºC and 750 ºC adsorbents (g). V is the solution volume of the methyl orange dye (L) [25].

Research Paper **© 2012 IJFANS. All Rights Reserved**

4. RESULT AND DISCUSSION

4.1 X-RAY DIFFRACTION

XRD analysis is a key technique for studying the crystalline structure, phase composition, and average particle size of SiO_2 nanoparticles synthesized from cassava periderm ash. This method offers critical information about the material's structural properties, which are essential for applications in electronics, optics, and catalysis [26]. The XRD pattern (Fig. 2) shows distinct diffraction peaks typical of a tetragonal structure, with Bragg angles (2θ) at 22.4°, 31.9°, 35.2°, 38.6°, 49.7°, 56.7° for 3N of CPA at 650 ºC and also 22.5°, 32.08°, 35.01°, 38.02°, 48.2°, 56.1° for 5N of CPA at 650 ºC. Similarly figure.2 shows the diffraction peaks typical of a tetragonal structure, with Bragg angles (2θ) at 21.6°, 30.8°, 35.3°, 38.1°, 48.9°, 56.6° for 3N of CPA at 750 ºC and also 21.7°, 31.0°, 35.°, 38.1°, 48.5°, 56.7° for 5N of CPA at 650 ºC. These peaks match the (141), (161), (170), (152), (300), and (310) crystallographic planes, as indicated by their Miller indices (hkl). The tetragonal structure is known for its excellent thermal and chemical stability [27]. The peak positions closely align with the standard JCPDS reference (file no. 39-0973), confirming the high purity SiO_2 nanoparticles. The absence of significant impurities ensures optimal performance in various applications. The average crystallite size was determined using the Scherrer equation, focusing on the most intense peak (141):

$D = k\lambda/\beta\cos\theta$

where: D is crystallite size, k is Scherrer's constant (0.94), λ is X-ray wavelength (0.15406 nm), β is peak width at half maximum (5 in radians), θ is Bragg angle (36.2°) [27]. The calculated crystallite size was approximately 28.8 nm for 650 ºC and 30.5 nm for 750 ºC, indicating a high surface area-to-volume ratio. This property enhances the nanoparticles' reactivity, making them suitable for applications such as photocatalysis and antimicrobial activity. The figure 2:(a-b) shows X-ray diffraction patterns of CPA prepared at different calcination temperatures 650 °C and its characteristic peak and also figure 2:(c-d) expects X-ray diffraction patterns of CPA prepared at different calcination temperatures 750 °C and its characteristic peak.

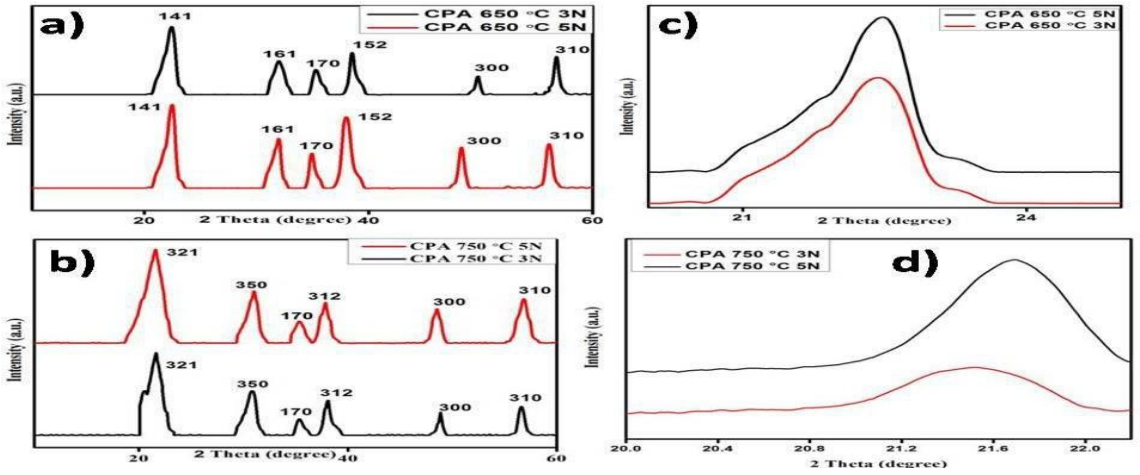

Fig 2: a-b: X-ray diffraction patterns of CPA prepared at different calcination temperatures 650 °C and its characteristic peak, c-d: X-ray diffraction patterns of CPA prepared at different calcination temperatures 750 °C and its characteristic peak.

Research Paper **© 2012 IJFANS. All Rights Reserved**

4.2 SCANNING ELECTRON MICROSCOPE

Scanning electron microscopy (SEM) was utilized to investigate the morphological features and particle size distribution of the synthesized materials, as shown in figures 3, the micrograph of CPA at 650 °C and CPA at 750 °C. In the CPA at 750 °C sample, the particles appeared relatively fine and well-dispersed, with sizes primarily ranging between 29 and 31 nm. The particles are mostly irregular in shape. Some of them look like small granules or sub-angular particles not perfectly round, not sharply edged either along with some needle like particles [28]. The structure looks a bit porous or rough-surfaced. Conversely, the CPA at 650 °C sample exhibited larger, more aggregated structures, with particle sizes predominantly in the range of 25 to 28 nm. The particles are also irregular, but they appear more aggregated and form larger clusters. Some larger formations have a flaky or plate-like texture. The surface seems a bit denser compared to CPA at 750 °C [29]. The observed difference in particle size and aggregation behavior between the two samples may be attributed to variations in synthesis conditions, leading to changes in nucleation and growth dynamics. These morphological characteristics are expected to significantly influence the surface area, porosity, and ultimately the functional performance of the materials in their intended applications [30]. The figure: 4 show the EDX spectrum and (a-c) depicts mapping of CPA silica synthesized at 750 ºC.

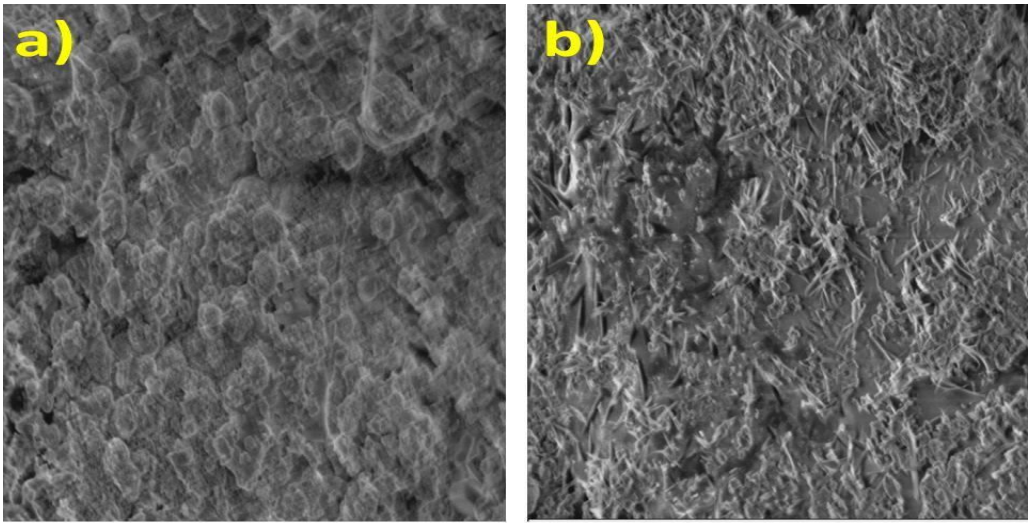

Fig 3: Different maginification of Scanning Electron Micrograph of a) CPA at 650ºC and b) CPA at 750 °C.

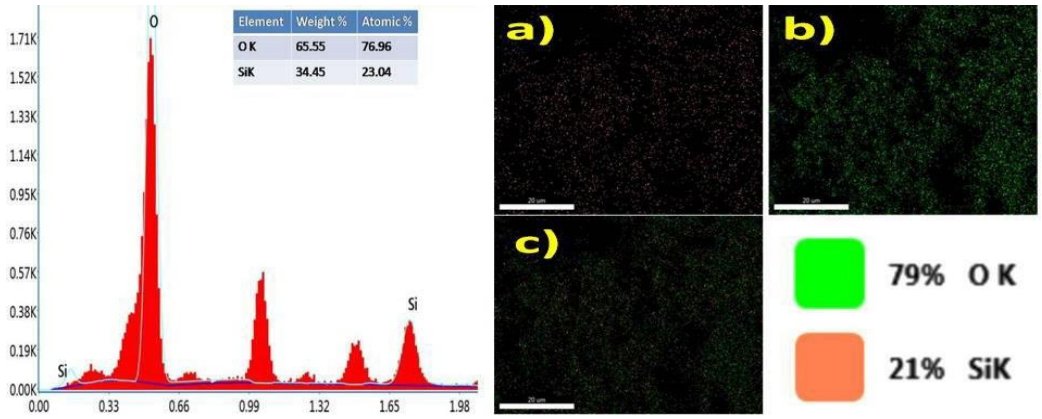

Fig.4: EDX spectrum and (a-c) mapping of CPA silica synthesized at 750 ºC

4.3 FTIR

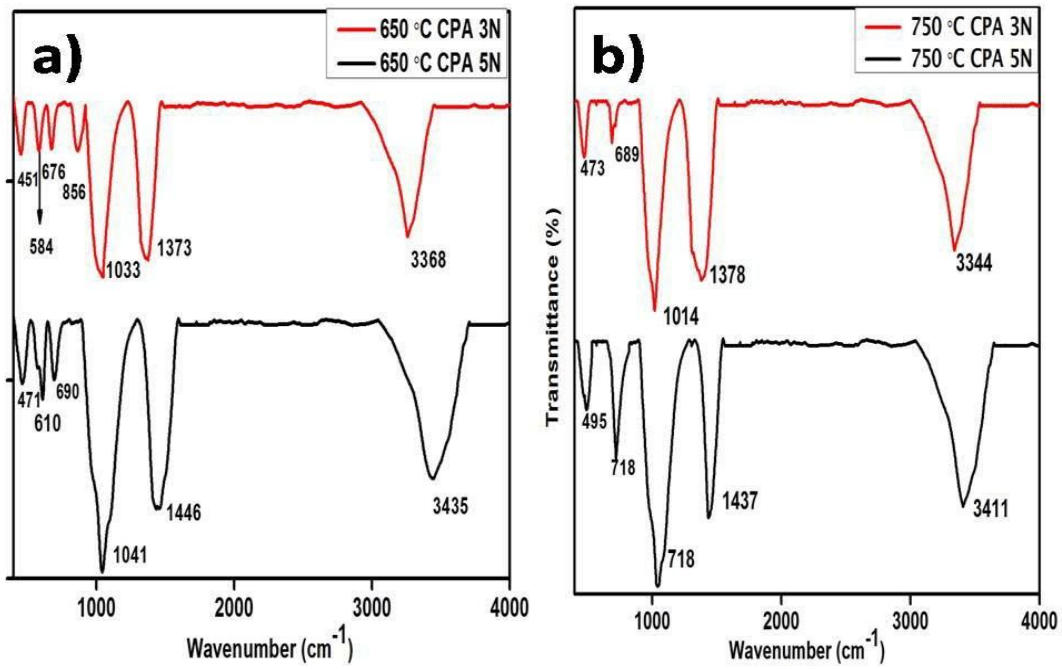

Fig 5: Fourier transform infrared spectra of synthesized CPA silica a) 650 °C and b) 750 °C

FTIR spectroscopy proved valuable in detecting residual pollutants in the samples and helped elucidate the structural changes occurring on the material's surface at varying temperatures. Researchers utilized FTIR to assess key characteristics such as the degree of polymerization, surface functional groups, and thermal modificationsin the silica structure. The primary spectral features observed in silica from CPA include: A strong peak near 1040 cm^{-1}, attributed to the Si–O–Si asymmetric stretching vibration, confirming the siloxane backbone of the silica network [31]. A broad band around 3400 cm^{-1}, corresponding to Si–OH (silanol) groups, indicating hydroxyl-terminated surfaces that enhance hydrophilicity and adsorption potential [32]. There are some additional characteristic peaks, such as: ~1090 cm^{-1} (Si–O–Si asymmetric stretch), ~800 cm^{-1} (Si–O–Si symmetric stretch), and ~ 960 cm^{-1} (Si–OH stretching vibration). These findings confirm the presence of hydrated silica surfaces, which facilitate dye adsorption through hydrogen-bonding interactions [33]. The silanol groups (Si–OH) play a critical role in surface reactivity, making the material effective for pollutant capture in water treatment applications. The presence of unreacted TEOS in the silica particles may be determined using the absorbtion bands 2980 cm^{-1} (CH3) and 2930 cm^{-1} (CH2). These bands were not seen since the process relies on the synthesis of silica from biomass [34]. The table: 1 shows the FTIR tentative frequency assignments of nano silica synthesized by the precipitation method.

Table 1: FTIR tentative frequency assignments of nano silica

SL.NO	BAND ASSIGNMENT	WAVE NUMBER (CM^{-1})			
		650 ºC		750 ºC	
01	Bending vibration of Si-O-Si	451	471	495	473
02	Symmetric stretching vibration bands of Si-O	676	690	718	689
03	Stretching vibration of	856	-	843	875

	Si-O-Si				
04	Asymmetric stretching mode of Si-O-Si	1035	1041	1044	1014
05	Bending vibration of water molecules	1373	1446	1437	1378
06	Twisting pattern vibration of H-O-H	3368	3435	3411	3344

4.4 Bet

All the high-quality calcined silica samples displayed characteristic type IV nitrogen adsorption–desorption isotherms, as illustrated in Figure 6. This is indicative of mesoporous materials. The two calcined samples showed distinct adsorption–desorption steps within the relative pressure (P/P_0) range of 0.4 to 1.0, which suggests the presence of two types of narrow mesopore size distributions [35]. A prominent capillary condensation step was observed around $P/P_0 \approx 0.45$, corresponding to uniform mesopores formed within the silica surface. In contrast, a second step near $P/P_0 \approx 0.95$ is likely associated with multilayer nitrogen adsorption occurring in larger, textural mesopores or interparticle voids [36]. Pore size distribution analysis further confirmed the uniformity of the mesopores, all showing a consistent Barrett–Joyner–Halenda (BJH) pore radius of approximately 19.108 Å for CPA 650 ºC and 21.08 Å for CPA 750 ºC [37]. The total pore volume of CPA 650 ºC is 0.030 cc/g and CPA 750 ºC is 0.019 cc/g. Additionally, the samples exhibited a high Brunauer–Emmett–Teller (BET) specific surface area of 483 m^2/g for CPA 650 ºC and 523 m^2/g for CPA 750 ºC, which is favorable for applications requiring high surface reactivity [38]. These textural characteristics not only confirm the successful formation of mesoporous structures but also suggest that the calcination process effectively preserved the pore architecture, which is critical for maintaining high surface accessibility and enhancing material performance in applications like photocatalysis, supercapacitors, or drug delivery [39]. The figure 6 shows the N_2 adsorption/desorption isotherms and BJH curve of the CPA synthesized at 650 ºC and 750 ºC.

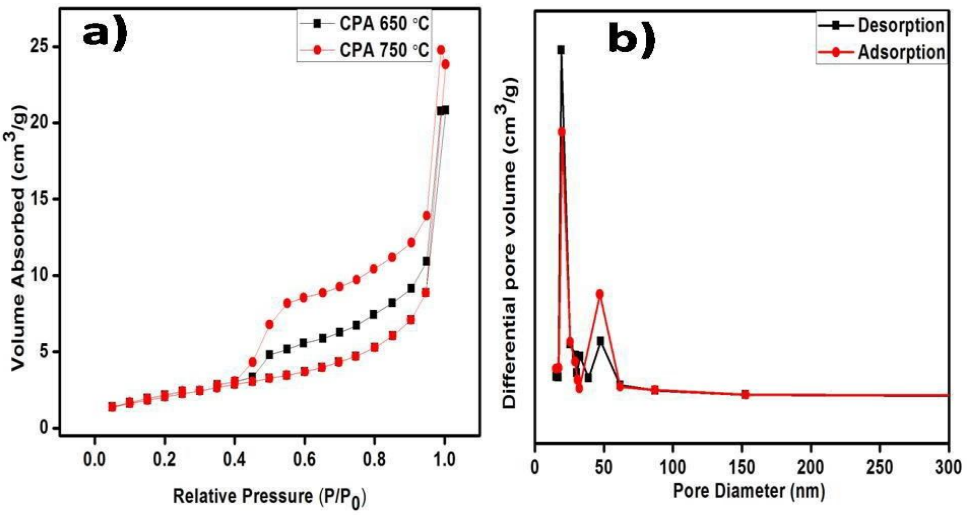

Fig 6: The N_2 adsorption/desorption isotherms and BJH curve of the CPA synthesized at 650 ºC and 750 ºC.

4.5 OPTICAL PROPERTIES

UV-visible (UV-Vis) spectroscopy is one of the most widely employed techniques for investigating the optical properties of materials, particularly nanoparticles. This method

involves measuring the absorption of light in the ultraviolet and visible regions of the electromagnetic spectrum. In this study, spectroscopic analysis was performed over the wavelength range of 250–500 nm [40]. The UV-Vis absorption spectrum, depicting optical absorbance as a function of wavelength, is presented in Figure 7. A prominent absorption peak was observed at approximately 300 - 320 nm, indicating the successful formation of SiO_2 nanoparticles [41]. The strong absorbance in the UV region suggests characteristic electronic transitions associated with nanoscale silica. Additionally, absorption in the visible range influences the apparent color of the material, which corresponds to electronic excitations between molecular orbitals [42].

To further analyze the optical band gap of the synthesized SiO_2, Tauc plots were constructed based on the UV-Vis data. The estimated band gap energies were found to be 1.08 eV for the sample calcined at 650 °C and 0.86 eV for the sample calcined at 750 °C [43]. The reduction in band gap with increasing calcination temperature may be attributed to enhanced crystallinity, particle growth, or slight changes in the structural ordering of the silica network [44]. These relatively low band gap values suggest that the materials could exhibit promising photocatalytic or optoelectronic properties under lower-energy (near-UV or visible) light irradiation. Furthermore, the sharp and well-defined absorption features, along with the band gap estimations, confirm the successful synthesis and optical activation of SiO_2 nanoparticles suitable for functional applications [45]. The figure:7 shows the Ultra violet absorption spectrum and tauc plot of CPA 650 ºC and 750 ºC.

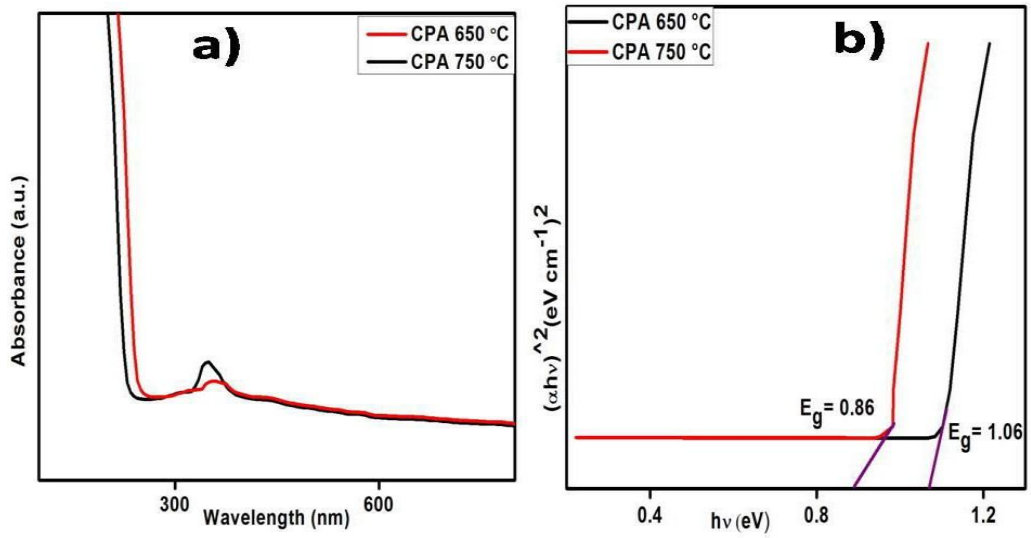

Fig 7: Ultra violet absorption spectrum and tauc plot of CPA 650 ºC and 750 ºC.

4.6 TEM

The TEM images of the SiO_2 NPs that were created are displayed in Figure 8. The homogeneous and aggregate spherical particles of CPA Silica vary in diameter from 25 to 30 nm. Silica particles combine to create a negatively charged colloidal gel under basic conditions. Strong electrostatic repulsive energy is induced by these colloidal particles to prevent agglomeration and gelation. A decreased distribution of SiO_2 NP states and particle aggregation via a Si-O-Si bridge were the outcomes of the desorption of other bio surfactant molecules in the CPA that had adsorbed on the surface of SiO_2 NPs during the synthesis process due to the high calcination temperature. Nevertheless, the use of a surfactant agent

Research Paper © 2012 IJFANS. All Rights Reserved

improved the particles' interfacial adhesion, which reduced agglomeration and increased dispersion [46].

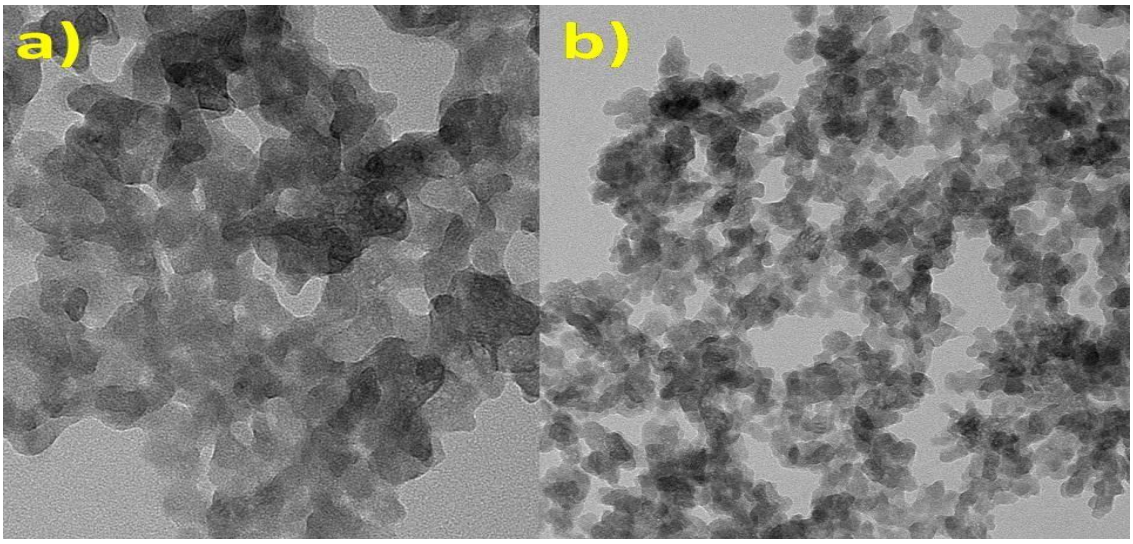

Fig 8: High-resolution transmission electron micrographs of CPA calcinated at 650 ºC and 750 ºC.

4.7 DISPOSAL OF METHYL ORANGE FROM AQUEOUS MEDIA

Crystalline silica demonstrates exceptional transparency to UVB, UVA, and visible light due to its wide bandgap (~9 eV), making it an effective host material for stabilizing and delivering drugs and dyes. However, structural defects and reduced crystallinity can lower its bandgap energy while simultaneously enhancing UV absorption. The highly reactive surface of silica, dominated by silanol (Si-OH) groups, facilitates the adsorption of both organic and inorganic compounds [47]. Under UV irradiation, silica nanoparticles (SiNPs) exhibit notable photocatalytic activity. This behavior stems from their ability to undergo photoexcitation, where charge transfer occurs from the SiO bonding orbital to the non-bridging oxygen 2p orbital, generating electron-hole pairs that drive photocatalytic reactions [40]. FTIR analysis confirms that the SiO^- and SiOH groups on the silica surface impart a negative charge, making SiNPs particularly effective at adsorbing cationic dyes [32]. When UV light interacts with SiO_2, electrons are excited from the valence band to the conduction band, leaving behind positively charged holes in the valence band. These charge carriers migrate to the surface, forming active photocatalytic sites that facilitate dye degradation [48].

Photocatalytic degradation studies examined the effect of varying SiNP concentrations (10–50 ppm) on methyl orange (MO) dye removal. At 50 ppm, SiNPs achieved 15% degradation within 20 minutes, whereas at 10 ppm, negligible degradation was observed similar to control experiments without SiNPs. This difference arises from insufficient adsorption sites at low SiNP concentrations relative to the dye concentration [49]. Optimal performance yielded 70% degradation within 90 minutes, demonstrating efficient photocatalytic activity. Temporal spectral changes in MO degradation at 650°C and 750°C are illustrated in Figure 9, highlighting the temperature-dependent efficacy of the process.

Research Paper © 2012 IJFANS. All Rights Reserved

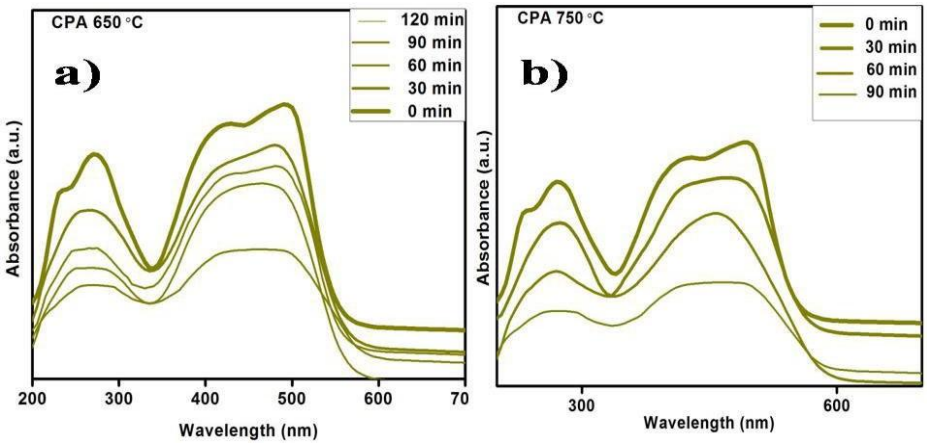

Fig 9: Temporal spectral changes of methyl orange in the a) 650 ºC b) 750 ºC

4.71 EFFECT OF VARIOUS PARAMETERS

The adsorption process is highly dependent on the pH of the dye solution, as it directly influences the surface charge of the adsorbent and the ionization state of the adsorbate molecules. Consequently, pH plays a crucial role in determining adsorption efficiency, particularly in systems where electrostatic interactions govern the process [50]. The ionization state of methyl orange and the surface charge of SiO_2 nanoparticles are both strongly impacted by the pH of the solution, which influences adsorption and degradation. The protonation of silanol groups, $\equiv Si–OH_2^+$, causes the SiO_2 surface to become positively charged at low pH. Electrostatic attraction causes methyl orange, an anionic dye, to absorb more strongly, accelerating degradation. But too much acidity can cause nanoparticles to aggregate, which lowers surface area and photocatalytic effectiveness. Although moderate adsorption takes place, decomposition could proceed more slowly than in acidic environments. Anionic dyes like MO degrade best at pH values between 4 and 6. The anionic MO dye is repelled by the negatively charged SiO_2 surface ($\equiv Si–O^-$), which decreases adsorption. At high pH, hydroxyl radicals (•OH) are more prevalent, although their effects can be countered by inadequate dye adsorption.In this study, the methyl orange(MO) dye removal efficiency of CPA 650 °C and CPA 750 °C adsorbents was evaluated across a pH range of 2 to 8. The experiments were conducted at room temperature for 3 hours using an initial MO concentration of 50 mg/L. To avoid complications from precipitation, tests were restricted to pH ≤ 8, as higher alkalinity promotes undesirable interactions. Methyl Orange, being a cationic dye, carries a positive charge in solution. At pH > 8, the increased hydroxide ion (OH^-) concentration can neutralize these positively charged dye molecules, leading to precipitation rather than adsorption [51]. As illustrated in Figure 10b, the removal efficiency of both adsorbents improved with increasing pH, demonstrating enhanced adsorption capacity under more alkaline conditions.

The adsorption efficiency of methyl orange (MO) dye was systematically evaluated across a temperature range of 25-80 °C using CPA 650 ºC and CPA 750 ºC adsorbents. Experiments were conducted at a fixed initial MO concentration (50 mg/L), pH 4, and contact time (150 min). As shown in Figure 10c, both adsorbents demonstrated significantly enhanced MO removal efficiency with increasing temperature, indicating an endothermic adsorption process. 50–60°C is ideal for improved kinetics without destabilizing nanoparticles. After

Research Paper © 2012 IJFANS. All Rights Reserved

70°C, efficiency decreases because of SiO_2 thermal aggregation. [52]. The study further investigated adsorption performance at varying MO concentrations (10-100 mg/L) under optimal conditions (pH 4, 90 min). Figure reveals two key trends: the absolute adsorption capacity increased with higher initial concentrations due to greater driving force and the percentage removal efficiency decreased at elevated concentrations, attributed to Saturation of active adsorption sites and reduced relative concentration gradient at higher initial loads. Because there are many active sites, the best efficiency occurs at low doses (10–20 mg/L). After 50 mg/L, efficiency drastically drops because to site saturation and light shielding. [53]. Finally after 120 minutes of irradiation, CPA -650 ºC achieved 64% MO degradation and CPA - 750 ºC showed superior performance with 70% degradation after 90 minutes.

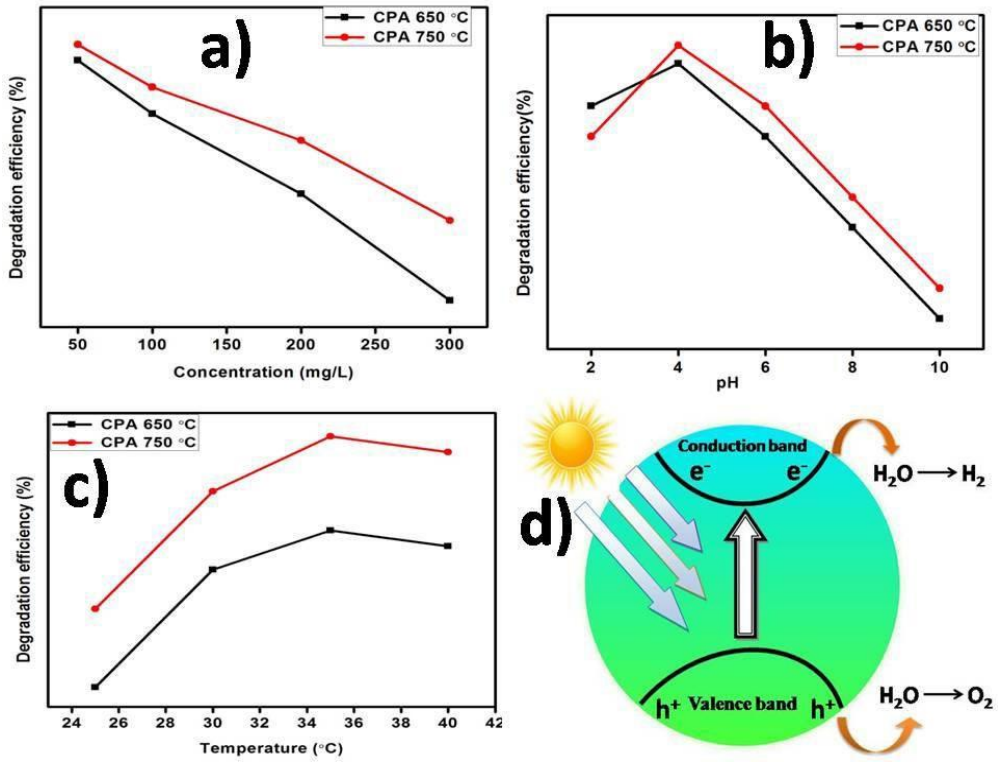

Fig 10: Effect of the a) temperature, b) pH, c) concentration on the % disposal of the methyl orange dye and d) mechanism of photocatalytic activity

CONCLUSION

Methyl orange (MO), a common organic dye found in industrial wastewater, can be effectively removed using silicon nanoparticles (SiNPs) synthesized from agricultural waste. This approach offers a dual advantage: repurposing agro-waste into a valuable resource and producing an eco-friendly, high-efficiency adsorbent for dye removal. SiNPs exhibit exceptional adsorption capabilities due to their high surface area, porosity, and surface reactivity, making them ideal for capturing organic pollutants. A promising source for SiNPs is Cassava Periderm ash, an underutilized agricultural byproduct. Converting this waste into functional nanoparticles aligns with the principles of circular economy, waste valorization, and sustainable development, reducing both environmental pollution and reliance on non-renewable materials. Agricultural waste is abundant and low-cost, making SiNP production economically viable. Their nanostructured surfaces provide numerous active sites for dye

Research Paper © 2012 IJFANS. All Rights Reserved

binding. SiNPs can be chemically functionalized to enhance selectivity for specific dyes. Unlike some conventional adsorbents, SiNPs are non-toxic and biodegradable. While SiNPs show excellent performance in organic dye removal, their efficiency in heavy metal adsorption from aqueous solutions requires further optimization. Future research could explore: hybrid nanocomposites (e.g., SiNPs combined with graphene oxide or chitosan) to improve adsorption kinetics, regeneration and reusability of SiNPs to enhance cost-effectiveness, large-Scale Applications in industrial wastewater treatment to assess feasibility under real world conditions. By leveraging agricultural waste-derived SiNPs, this method presents a sustainable, scalable, and eco-friendly solution for mitigating water pollution caused by synthetic dyes.

REFERENCE

1) Zarei, V.; Mirzaasadi, M.; Davarpanah, A.; Nasiri, A.; Valizadeh, M.; Hosseini, M.J.S., (2021). Environmental method for synthesizing amorphous silica oxide nanoparticles from a natural material. Processes 2021, 9, 334.

2) Chun, J.; Lee, J.H., (2020). Recent Progress on the Development of Engineered Silica Particles Derived from Rice Husk. Sustainability, 12, 10683. https://doi.org/10.3390/su122410683.

3) Karande, S.D.; Jadhav, S.A.; Garud, H.B.; Kalantre, V.A.; Burungale, S.H.; Patil, P.S., (2021). Green and sustainable synthesis of silica nanoparticles. Nanotechnol. Environ.Eng. 2021, 6, 29. https://doi.org/10.1007/s41204-021-00124-1.

4) Anuar, M.F.; Fen, Y.W.; Zaid, M.H.M.; Matori, K.A.; Khaidir, R.E.M.,(2018). Synthesis and structural properties of coconut husk as potential silica source. Results Phys. 2018, 11, 1–4. https://doi.org/10.1016/j.rinp.2018.08.018.

5) Nguyen, H.X.; Dao, N.T.T.; Nguyen, H.T.T.; Le, A.Q.T., (2019). Nanosilica synthesis from rice husk and application for soaking seeds. IOP Conf. Ser. Earth Environ. Sci. 2019, 266, 012007. doi :10.1088/1755-1315/266/1/012007.

6) Azat, S.; Sartova, Z.; Bekseitova, K.; Askaruly, K., (2019). Extraction of high-purity silica from rice husk via hydrochloric acid leaching treatment. Turk. J. Chem. 2019, 43, 1258–1269. Doi: 10.3906/kim-1903-53.

7) Akhayere, E.; Vaseashta, A.; Kavaz, D., (2020). Novel Magnetic Nano Silica Synthesis Using Barley Husk Waste for Removing Petroleum from Polluted Water for EnvironmentalSustainability. Sustainability 2020, 12,10646.https://doi.org/10.3390/su122410646.

8) Guo, W.; Li, G.; Zheng, Y.; Li, K., (2021). Nano-silica extracted from rice husk and its application in acetic acid steam reforming. RSC Adv. 2021, 11, 34915–34922. https://doi.org/10.1039/D1RA05255A.

9) Abdul Razak, N.A., Othman, N.H., Shayuti, M.S.M., Jumahat, A., Sapiai, N., Lau, W.J., (2022). Agricultural and industrial wastederived mesoporous silica nanoparticles: a review on chemical synthesis route. J. Environ. Chem. Eng. 10, (2). https://doi.org/ 10.1016/j.jece.2022.107322 107322.

10) Aashikha Shani, R.S., Jeice, A.R. Introspect of prying out silica from agricultural wastes by various methods and incorporating them in distinct uses. Biomass Conv. Bioref. (2024). https://doi.org/10.1007/s13399-024-05360-4.

Research Paper **© 2012 IJFANS. All Rights Reserved**

11) Chundawat, N.S., Parmar, B.S., Deuri, A.S., Vaidya, D., Jadoun, S., Zarrintaj, P., Barani, M., Chauhan, N.P.S., (2022). Rice husk silica as sustainable filler in the tire industry. Arab. J. Chem. 15, (9). https://doi.org/10.1016/j.arabjc.2022.104086 104086.

12) Osman NS, Sapawe N., (2020). Preparation of amorphous oil palm frond ash (OPFA) via acid leaching treatment as precursor for silica synthesis. Materials Today Proceedings. Elsevier, Amsterdam, pp 253–256. https://doi.org/10.1016/j.matpr.2020.05.333.

13) Adepoju, A.D., Adebisi, J.A., Odusote, J.K., Ahmed, I.I., Hassan, S.B., (2016). Preparation of Silica from Cassava Periderm. J. Solid Waste Technol. Manag. 42(3), 216–221 (2016). doi:10.5276/ JSWTM.2016.216.

14) Agbenyeku, E.-O. E., & Aneke, I. F., (2014). Prolonged Curing of Green Concrete from Domestically Derived Cassava Peels Ash (DDCPA) and Laterite. International Journal of Scientific & Engineering Research, Volume 5(1), pp. 900-905.

15) Joabel Raabe, Alessandra de Souza Fonseca, Lina Bufalino,Caue Ribeiro, Maria Alice Martins, JoséManoelMarconcini, Lourival M. Mendes, and Gustavo Henrique Denzin Tonoli., (2015). Biocomposite of Cassava Starch Reinforced with Cellulose Pulp Fibers Modified with Deposition of Silica (SiO_2) Nanoparticles. Hindawi Publishing Corporation Journal of Nanomaterials Volume 2015, Article ID 493439, 9 pages. http://dx.doi.org/10.1155/2015/493439.

16) Kurniawan, A., Kosasih, A. N., Febrianto, J., Ju, Y.-H., Sunarso, J., Indraswati, N., & Ismadji, S., (2011). Evaluation of cassava peel waste as lowcost biosorbent for Ni-sorption: Equilibrium, kinetics, thermodynamics and mechanism. Chemical Engineering Journal, Volume 172(1), pp. 158-166.

17) Mota-Guttierez, Jatziri; O'Brien, Gerard Michael (September 2019). Cassava consumption and the occurrence of cyanide in cassava in Vietnam, Indonesia and Philippines. Public Health Nutrition. Volume: 23 (13): 2410–2423. PMID 32438936., doi:10.1017/S136898001900524X. PMC 11374567.

18) Ebunilo, P., Egware, H. and Ukwuaba, S. (2013): Design and testing of an experimental cassava tuber peeling machine. International Journal of Engineering Research in Africa. 9(24), 35-42.

19) Priscila G.F., Moraes-Dallaqua, M.A., Bicudo, S.J. and Tanamati, F.Y. (2013): Starch accumulation in cassava roots: Spatial and temporal distribution. African Journal of Agricultural Research 8(46), 5712-5715.

20) Arisa N.U., Kadiri A.B. And Aworh O.C., (2016). Comparative anatomical evidence of the effects of two peeling methods on cassava (manihot esculenta crantz) roots. Journal of Industrial Research and Technology. JIRT Vol. 5 No 1, 2016.

21) Yuxin Liu, Lilan Fan, Junmei Xiong and Zesheng Liang., (2020). Effects of different particle size of silica on structure, morphology, and properties of thermoplastic cassava starch, Polymers and Polymer Composites 1–13 DOI: 10.1177/0967391120939664.

22) Bomfim N., Nassar.N.M.A., (2014). Development of cassava periclinal chimera may boost production. Genetics and Molecular Research 13 (1): 819-830. DOI: http://dx.doi.org/10.4238/2014.February.10.1.

Research Paper © 2012 IJFANS. All Rights Reserved

23) Aashikha Shani, R.S., Rejo Jeice, A., 2023. Articulate Synthesis of Nano Silica from coconut fibre by precipitation method. National Conference on Advances in materials Science. ISBN: No. 978-93-5811-124-8.
24) Jung.H, Kwak. H, Chun.J, and Oh. K., (2018). Characteristics of crystalline silica (SiO_2) particles prepared by simple solution method using sodium silicate (Na_2SiO_3) precursor. Journal of Physics: conference Series, 2018. nSci, 11 (2021), p. 10363, 10.3390/app112110363.
25) Nayak, P.; Datta, A. Synthesis of SiO_2-nanoparticles from rice husk ash and its comparison with commercial amorphous silica through material characterization. Silicon 2022, 12.
26) Zareihassangheshlaghi, A.; Beidaghy Dizaji, H.; Zeng, T.; Huth, P.; Ruf, T.; Denecke, R.; Enke, D. Behavior of metal impurities on surface and bulk of biogenic silica from rice husk combustion and the impact on ash-melting tendency. ACS Sustain. Chem. Eng. 2020, 8, 10369–10379.
27) Kumar, A.; Bera, S.; Singh, M.; Mondal, D., (2021). Molecular Interactions of Silica Nanoparticles and Biomolecule-Functionalized Silica Nanoparticles with Bixa orellana L. Plant DNA. Silicon 2021, 14, 1407–1419.
28) Nassar, M.Y.; Ahmed, I.S.; Raya, M.A.Afacile and tunable approach for synthesis of pure silica nanostructures from rice husk for the removal of ciprofloxacin drug from polluted aqueous solutions. J. Mol. Liq. 2019, 282, 251–263.
29) Rajan, R.; Zakaria, Y.; Shamsuddin, S.; Hassan, N.F.N. Robust synthesis of mono-dispersed spherical silica nanoparticle from rice husk for high definition latent fingermark development. Arab. J. Chem. 2020, 13, 8119–8132.
30) Hwang, J.; Lee, J.H.; Chun, J. Facile approach for the synthesis of spherical mesoporous silica nanoparticles from sodium silicate. Mater., Lett. 2021, 283, 128765.
31) Huei Ruey Onga., Wan Mohd Eqhwan Iskandara, Jason Chonga, Md. Maksudur Rahman Khanb, Thai Kiat Ongc , Beng Kooi Chuad., Investigation on Silane Concentration of SiO_2 Nanoparticle: FTIR Analysis Chemical Engineering Transactions, 106, 1345-1350 ., CHEMICAL ENGINEERING TRANSACTIONS VOL. 106, (2023) DOI:10.3303/CET23106225.
32) Qu, G.; Han, Y.; Qi, J.; Xing, X.; Hou, M.; Sun, Y.;Wang, X.; Sun, G. Rapid iodine capture from radioactive wastewater by green and low-cost biomass waste derived porous silicon–carbon composite. RSC Adv. 2021, 11, 5268–5275.
33) Ruth Ellerbrock, Mathias Stein & Jörg Schalle., Comparing amorphous silica, Short range ordered silicates and silicic acid species by FTIR. Scientific Reports | (2022) 12:11708. https://doi.org/10.1038/s41598-022-15882-4.
34) Kaya, H., Ngo, D., Gin, S. & Kim, S. H., (2020). Spectral changes in Si–O–Si stretching band of porous glass network upon ingress of water.J. Non-Cryst. Solids 527, 119722.
35) Chun, J.; Gu, Y.M.; Hwang, J.; Oh, K.K.; Lee, J.H., (2020). Synthesis of ordered mesoporous silica with various pore structures using high-purity silica extracted from rice husk. J. Ind. Eng. Chem. 2020, 81, 135–143.

36) Samy.A, Ismail.A.M, and Heba Ali., (2023). Environmentally friendly mesoporous SiO_2 with mixed fiber/particle morphology and large surface area for enhanced dye adsorption. J Mater Sci Composites & nanocomposites 58:1586–1607. https://doi.org/10.1007/s10853-022-08119-2.

37) Norzahir Sapawe, Nor Surayah Osman, Mohd Zulkhairi Zakaria, Syed Amirul Shahab Syed Mohamad Fikry, Muhammad Amir Mat Aris., 2018. Synthesis of green silica from agricultural waste by sol-gel method. Materials today proceedings 5, 10, 2, 21861-21866. https://doi.org/10.1016/j.matpr.2018.07.043.

38) Purnawira, B.; Purwaningsih, H.; Ervianto, Y.; Pratiwi, V.; Susanti, D.; Rochiem, R.; Purniawan, A., (2019). Synthesis and characterization of mesoporous silica nanoparticles (MSNp) MCM 41 from natural waste rice husk. IOP Conf. Ser., Mater. Sci. Eng. 2019, 541, 012018.

39) Davarpanah, J.; Sayahi, M.H.; Ghahremani, M.; Karkhoei, S., (2019). Synthesis and characterization of nano acid catalyst derived fromrice husk silica and its application for the synthesis of 3, 4-dihydropyrimidinones/thiones compounds. J. Mol. Struct. 2019, 1181, 546–555.

40) Patrick Ehi Imoisili and Tien-Chien Jen, 2021. Facile extraction and characterization of Silica nanoparticles from Corn Stalk by Sol Gel Hydrothermal methods. International Conference on Engineering for Sustainable World (ICESW 2020) IOP Conf. Series: Materials Science and Engineering 1107- 012030 IOP Publishing. doi:10.1088/1757-899X/1107/1/012030.

41) Ahmad Alyosef, H.; Schneider, D.; Wassersleben, S.; Roggendorf, H.; Weiß, M.; Eilert, A.; Denecke, R.; Hartmann, I.; Enke, D. Meso/macroporous silica from miscanthus, cereal remnant pellets, and wheat straw. ACS Sustain. Chem. Eng. 2015, 3, 2012–2021.

42) Amirhossein Zareihassangheshlaghi., Hossein Beidaghy Dizaji., Thomas Zeng., Paula Huth., Thomas Ruf., Reinhard Denecke., Dirk Enke., 2020. The behaviour of metal impurities on surface and bulk of biogenic silica from rice husk combustion and their impact on ash melting tendency. ACS Sustainable Chemistry & Engineering. Page 1-26. DOI:10.1021/acsuschemeng.0c01484

43) Fu, L.; Zhu, J.; Huang, W.; Fang, J.; Sun, X.; Wang, X.; Liao, K., (2020). Preparation of Nano-Porous Carbon-Silica Composites and Its Adsorption Capacity to Volatile Organic Compounds. Processes 2020, 8, 372.

44) Ebnalwaled, A.A.; Sadek, A.H.; Ismail, S.H.; Mohamed, G.G. Structural, optical, dielectric, and surface properties of polyimide hybrid nanocomposites films embedded mesoporous silica nanoparticles synthesized from rice husk ash for optoelectronic applications. Opt. Quantum Electron. 2022, 54, 690.

45) Elchin Huseynova,Adil Garibova, Ravan Mehdiyevab (2015) TEM and SEM study of nano SiO2 particles exposed to influence of neutron flux**.** Journal of materials research and technology, 5(3):213–218.

46) El-Hakam, S.A.; Al-Shorifi, F.T.; Salama, R.S.; Gamal, S.; El-Yazeed, W.S.A.; Ibrahim, A.A.; Ahmed, A.I. Application of nanostructured mesoporous silica/ bismuth vanadate composite catalysts for the degradation of methylene blue and brilliant green. J. Mater. Res. Technol. 2022, 18, 1963–1976. https://doi.org/10.1016/j.jmrt.2022.03.067.

47) Borhade .A.V, Tope.D.R, and Gite.S.G., (2017). Synthesis, characterization and catalytic application of silica supported tin oxide nanoparticles for synthesis of 2, 4, 5-tri and 1, 2, 4, 5-tetrasubstituted imidazoles under solvent-free conditions, Arabian Journal of Chemistry, vol. 10, pp. S559–S567, 2017.

48) Liu.J, Ma.S, and Zang.L, (2013). Preparation and characterization of ammonium-functionalized silica nanoparticle as a new adsorbent to remove methyl orange from aqueous solution, Applied Surface Science, vol. 265, pp. 393–398, 2013.

49) Prado-Chay, D.A.; Cortés-Jácome, M.A.; Angeles-Chávez, C.; Oviedo-Roa, R.; Martínez-Magadán, J.M.; Zuriaga-Monroy, C.;Hernández-Hernández, I.J.; Mayoral, P.R.; Gómora-Herrera, D.R.; Toledo-Antonio, J.A., (2020). Synthesis and Photocatalytic Activity of Cu_2O Microspheres upon Methyl Orange Degradation. Top. Catal. 2020, 63, 586–600.

50) Al-Baldawi, I.A.; Abdullah, S.R.S.; Almansoory, A.F.; Ismail, N.I.; Hasan, H.A.; Anuar, N., (2020). Role of Salvinia molesta in biodecolorizationof methyl orange dye from water. Sci. Rep. 2020, 10, 13980.

51) Safavi-Mirmahalleh, S.-A.; Salami-Kalajahi, M.; Roghani-Mamaqani, H., (2020), Adsorption kinetics of methyl orange from water by pH-sensitive poly (2-(dimethylamino)ethyl methacrylate)/nanocrystalline cellulose hydrogels. Environ. Sci. Pollut Res. 2020, 27, 28091–28103.

52) El-Shamy, A.G., (2022). Novel in-situ synthesis of nano-silica (SiO_2) embedded into polyvinyl alcohol for dye removal: Adsorption and photo-degradation under visible light. Polymer 2022, 242, 124579.

53) Pratibha Sharma, Jaibir Kherb, Jai Prakash, Raj Kaushal., 2021. A novel and facile green synthesis of SiO_2 nanoparticles for removal of toxic water pollutants. Applied Nanoscience, 13, 735–747. http://dx.doi.org/10.1007/s13204-021-01898-1.